Photochemistry of the Primary Event in Short-Wavelength Visual Opsins at Low Temperature†

Bryan W. Vought,‡ Abhiram Dukkipatti,‡ Marianna Max,§ Barry E. Knox,|| and Robert R. Birge*,‡

Departments of Chemistry and Biology, Syracuse University, 111 College Place, Syracuse, New York 13244-4100, Department of Physiology and Biophysics, Mount Sinai School of Medicine, New York, New York 10029, and Department of Biochemistry and Molecular Biology, SUNY Health Science Center, 750 East Adams Street, Syracuse, New York 13210

Received April 28, 1999; Revised Manuscript Received June 9, 1999

ABSTRACT: Two short-wavelength cone opsins, frog (*Xenopus laevis*) violet and mouse UV, were expressed in mammalian COS1 cells, purified in delipidated form, and studied using cryogenic UV−vis spectrophotometry. At room temperature, the *X. laevis* violet opsin has an absorption maximum at 426 nm when generated with 11-*cis*-retinal and an absorption maximum of 415 nm when generated with 9-*cis*-retinal. The frog short-wavelength opsin has two different batho intermediates, one stable at 30 K ($\lambda_{max} \approx 446$ nm) and the other at 70 K ($\lambda_{max} \approx 475$ nm). Chloride ions do not affect the absorption maximum of the violet opsin. At room temperature, mouse UV opsin has an absorption maximum of 357 nm, while at 70 K, the pigment exhibits a bathochromic shift to 403 nm with distinct vibronic structure and a strong secondary vibronic band at 380 nm. We have observed linear relationships when analyzing the energy difference between the initial and bathochromic intermediates and the normalized difference spectra of the batho-shifted intermediates of rod and cone opsins. We conclude that the binding sites of these pigments change from red to green to violet via systematic shifts in the position of the primary counterion relative to the protonated Schiff base. The mouse UV cone opsin does not fit this trend, and we conclude that wavelength selection in this pigment must operate via a different molecular mechanism. We discuss the possibility that the mouse UV chromophore is initially unprotonated.

Photopic vision is mediated by cone cells, which function at high levels of illumination, respond to rapid changes in light, and permit color discrimination (*1*). The spectral sensitivity of cone cells is determined by expression of a particular cone opsin, a member of a larger family of visual pigments that bind 11-*cis*-retinal to form the phototransduction protein. The cone opsins are subdivided into groups according to their amino acid similarity, as shown in the dendogram in Figure 1 [adapted from the work of Yoshizawa (*2*) and Yokoyama (*3*)]. The vertebrate opsins are divided by amino acid homology into five groups: cone opsin groups S, M_1, M_2, and L and the (rod) rhodopsins (*4*). Each group exhibits a different wavelength region of maximum extinction, suggesting that the mechanisms for wavelength regulation in the cone pigments have been a major factor in the evolution of these proteins (*3*−*5*). The actual names assigned to the cone pigments do not necessarily correspond to the color classifications, because some protein names were assigned before the classification scheme shown in Figure 1 was developed. For example, group S (UV-violet cone opsins) includes both the *Xenopus laevis* (frog) violet and the human blue cone opsins.

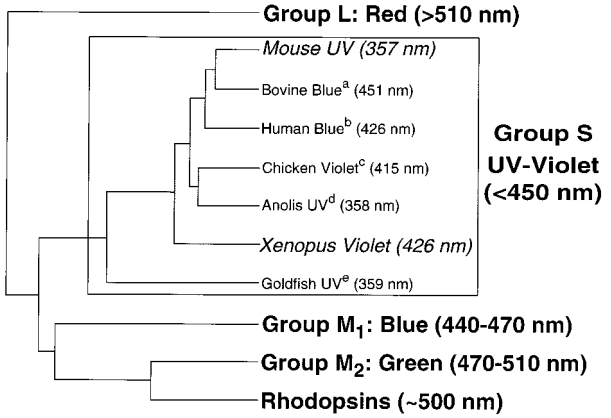

FIGURE 1: Dendogram showing the amino acid similarities among the visual pigments. Seven short-wavelength visual pigments and representative sequences of other visual pigments were compared using the PILEUP program (GCG9, Madison, WI). The sequences group according to wavelength properties. Note that the names assigned to the pigments do not necessarily agree with their absorption maxima. The values in parentheses correspond to the maximum absorbance (λ_{max}) for each of the pigments: footnote *a*, ref *8*; footnote *b*, ref *23*; footnote *c*, ref *20*; footnote *d*, ref *24*; footnote *e*, refs *7* and *54*.

One of the fundamental questions in current vision research concerns the nature of the protein−chromophore interactions and how these interactions influence the photophysical properties of the chromophore. The short-wavelength pigments pose a particular challenge in the understanding of retinal−protein interactions, because many of the absorp-

† This work was supported in part by NIH Grants GM 34548, EY 09409, and EY 11256.

* To whom correspondence should be addressed. Tel: 315-443-1900. Fax: 315-443-4070. E-mail: rbirge@syr.edu.

‡ Syracuse University.

§ Mount Sinai School of Medicine.

|| SUNY Health Science Center.

10.1021/bi990968b CCC: $18.00
Published on Web 08/13/1999

tion spectra are blue-shifted compared to a solvated protonated Schiff base (λ_{max} = 440 nm), unlike the red-shifted green and red absorbing pigments (*6*). Furthermore, the range of absorption maxima of the group S pigments is much greater (~100 nm) than for any of the other groups (~40 nm). For example, the two most closely related opsins in Figure 1, the mouse UV (λ_{max} = 357 nm) (*7*) and bovine blue cone opsins (λ_{max} = 451 nm) (*8*), are 89% identical (*9*) and 94% similar (*10*) but differ by 94 nm in their absorption maxima. On the basis of amino acid sequence comparisons, the group S pigments do not segregate according to absorption maximum (e.g., UV, violet, and blue λ_{max} together). Although many investigators have emphasized the role individual residues have on spectral tuning (e.g., refs *11*−*17*), there are currently no adequate explanations for spectral tuning in this group or how these pigments evolved.

The retinal binding site of short-wavelength cone opsins remains an area of speculation. Experimental studies have been hindered by two factors. First, isolating the UV/violet cone opsins from retinas in quantities sufficient for spectroscopic studies is difficult, due to the relatively low abundance (*18*, *19*). Second, lipids used to stabilize cone pigments scatter light at cryogenic temperatures, making UV−vis spectroscopy of UV/violet-absorbing proteins nearly impossible (*20*). Some S-group cone opsins have been expressed previously [human blue opsin (*21*−*23*), the anolis UV opsin (*24*), the UV opsins from mouse, rat, pigeon, and goldfish (*7*), and budgerigar (*15*)]. Previous work has shown that *X. laevis* violet cone opsin cDNA can be expressed in COS1 cells and purified using immunoaffinity chromatography (*10*, *25*). When this pigment is generated using 11-cis A_1 retinal, the absorption maximum is 425 ± 1 nm, identical to the human blue cone opsin (*22*, *26*).

The violet cone opsin from *X. laevis* is stable when solubilized in *N*-dodecyl β-D-maltoside (LM),[1] making it an ideal candidate for extensive biophysical studies (*10*, *25*). In this study we express the mouse UV cone opsin in COS1 cells and solubilize it in LM, free of any lipids. We then study the properties of the primary (batho) intermediates of the violet and UV cone opsins by combining cryogenic spectroscopy and photostationary state formation with chromophore extraction and quantitation. Through a comparison of the batho-intermediate data from these pigments with those of other vertebrate pigments, we postulate that the spectral tuning of these opsins is mediated by the selective placement of a single Asp or Glu counterion in proximity to the protonated Schiff base. We suggest on the basis of oscillator strength trends that spectral tuning in the mouse UV cone opsin operates via a different molecular mechanism.

MATERIALS AND METHODS

Construction of the Mouse UV Expression Vector. The expression vector pMT-VCOP has been described previously (*25*). The expression vector pMT-MUV was constructed for the transient expression of the mouse UV opsin cDNA in mammalian COS1 cells (*27*). A cDNA containing amino acids 1−325 of mUV opsin was amplified by PCR using a mouse cDNA clone as template (*9*). The forward primer, 5′-CAAGAATTCCACC**ATG**TCAGGAGAGGATG-3′, contained an *Eco*RI linker (underlined), a Kozak concensus sequence (CCACC), and the first 16 nt of the coding region (initiation codon in bold). The reverse primer, 5′-CGCGTGTCGACGCAGATTCGTCTGC-3′, contained a *Sal*I site (underlined) to permit cloning into the synthetic bovine rhodopsin gene (*27*). PCR was carried out, and the product was digested with *Eco*RI and *Sal*I and subcloned into the pMT expression vector (*28*). The resulting plasmid contained a cDNA encoding a fusion protein of 341 amino acids (1−325 from the mouse UV opsin and 333−348 plus the stop codon from the bovine rhodopsin gene) and the binding site for the monoclonal antibody 1D4 (*29*). Both strands of the coding region from pMT-MUV were sequenced.

Expression and Purification of X. laevis Violet and Mouse UV Cone Opsins. The expression vector pMT-VCOP or pMT-MUV was transiently transfected into mammalian COS1 cells as previously described (*10*). The visual pigments were purified by batchwise immunoaffinity chromatography on 1D4-Sepharose (*27*). 1D4 IgG was obtained from the Cell Culture Center and National Center for Research Resources (Minneapolis, MN), and 11-*cis*-retinal was provided by the NEI (via Rosalie Crouch). The washing and elution were performed in buffer W [buffer Y1 containing 0.1% LM and 20% (w/v) glycerol], and the pigment was eluted from the 1D4-Sepharose with two successive incubations with 0.5−1 mL of 40 μM competing peptide in buffer W. Chloride-free violet opsin was washed while it was bound to the 1D4-Sepharose beads with 10 bed volumes of 50 mM HEPES and 150 mM sodium gluconate, pH 6.6. Sodium gluconate was used rather than doubly distilled H_2O to minimize protein denaturation (*30*). The eluted material was concentrated with a Centricon C-30 (Amicon) and stored on ice. The average yield was 4 μg of violet opsin and 1.5 μg of UV opsin per 15 cm plate transfected. Bovine rhodopsin was purified from ROS as described (*31*).

Low-Temperature Spectroscopy of Solubilized Rhodopsin, the Violet Cone Opsin, and the UV Cone Opsin. We modified our Air Products Displex helium refrigerator cold tip so that a small-volume sample cell could be used. Photoconversion of the pigments was performed with either (for wavelengths less than 415 nm) a 100 W HgXe arc lamp through a monochromator and a 5 cm water cell to absorb heat or (for wavelengths greater than 415 nm) a Coherent Infinity/XPO tunable laser. Coupling optics maximized illumination of the sample while in the cold tip. Protein samples contained 67% glycerol, 0.05% LM, and buffer Y1. The samples were thermally equilibrated at 70 K for 1 h and then illuminated with blue light relative to the absorption maximum of the pigment (437 nm for bovine rhodopsin, 395 nm light for the violet opsin, and 305 nm for mouse UV opsin) to generate a maximum amount of the bathochromic photoproduct. Then, red light relative to the absorption maximum (565 nm for bovine rhodopsin, 500 nm for violet opsin, and 405 nm for UV opsin) was used to generate the reverse photostationary state.

Retinal Extraction and HPLC Analysis. After illumination at 70 K, the protein samples were removed from the cold tip in the dark and warmed to 0 °C. Unless otherwise

[1] Abbreviations: HEPES, *N*-(2-hydroxyethyl)piperazine-*N*′-2-ethanesulfonic acid; LM, *N*-dodecyl β-D-maltoside; PSS*xyz*, photostationary state generated at wavelength *xyz* nm; ROS, rod outer segments; WT, wild type.

Table 1: Spectroscopic and Chromophore Extraction Properties of Bovine Rhodopsin

	T (K)	λ_{max} (nm)	ϵ (M^{-1} cm^{-1})	$\Delta\nu_{FWHM}$ (cm^{-1})	f [a]	ρ [a]	11-cis	all-trans	9-cis
WT (lit.)[b]	277	500	40700	4250	0.98	1.86			
WT	277	500		4220	0.99				
WT	70	505		3785		1.80	95	5	0
PSS458	70	515		3970			28	58	14
PSS458[c]	70						28	58	14
PSS565	70	498					11	2	87
PSS565[c]	70						8	1	91

[a] f is oscillator strength and ρ is skewness, a dimensionless parameter which is an indirect measure of the distribution of vibronic activity into higher vibrational modes due to Franck−Condon activity (*53*). [b] Reference *53*. [c] References *37* and *38*.

specified, all extraction procedures were done in the dark or under dim red light with ice-cold solvents. The retinals were extracted in dichloroethane as oximes to stabilize their isomeric configuration using previously reported methods (*32*, *33*). To the 800 μL sample of glycerol/protein were added 100 μL of 1.0 M hydroxylamine (pH 7.0), 1 mL of methanol, and 1 mL of dichloroethane. The solution was shaken vigorously for 60 s and put on ice. Then, 5 mL of hexane was added, and the sample was shaken and spun in a clinical centrifuge for 45 s. The hexane layer was removed, and another 5 mL hexane extraction was performed. Anhydrous magnesium sulfate was added to the combined hexane layers. The hexane was then filtered through a 0.2 μm filter and evaporated in a different tube under vacuum. Finally, the retinal extract was brought up in 40 μL of hexane, and 20 μL was loaded onto the HPLC.

The HPLC methods used were similar to those described by Landers and Olson (*34*). A Waters DeltaPrep 4000 HPLC was used with a model 2487 detector monitoring at 360 nm. Two Waters 3.9 × 300 mm Prep NovaPak HR silica columns (WAT038051) were used in series. The isocratic mobile phase was filtered, sparged with helium, and composed of HPLC solvent grade hexane [96% (v/v)], ethyl acetate (3%), 1-octanol (0.5%), and 1,4-dioxane (0.5%). The relative isomeric concentrations of retinal oximes were determined by using the chromatogram peak areas and the retinal oxime extinction coefficients in hexane at 360 nm: 11-cis (anti) = 29 600 M^{-1} cm^{-1}, all-trans (anti) = 51 600 M^{-1} cm^{-1}, and 9-cis (anti) retinal oxime = 30 600 M^{-1} cm^{-1} (*32*, *35*).

Retinal oxime standards were made by individually combining *all-trans*-retinal (Fisher Scientific), 9-*cis*-retinal (Fisher Scientific), and 11-*cis*-retinal (from NEI, via Rosalie Crouch) with one-tenth volume of 1 M hydroxylamine (pH 7.0) in ice-cold methanol. The retinal oximes were then extracted with two 5 mL aliquots of hexane as described above. The hexane was then dried over anhydrous magnesium sulfate and evaporated under vacuum before being brought up to volume in hexane.

RESULTS

Low-Temperature Spectroscopy of Bovine Rhodopsin. Rhodopsin was studied first because the photostationary states of rhodopsin have been well characterized in the literature (*36*, *37*), and we sought to confirm that rhodopsin solubilized in LM would exhibit spectroscopic and photochemical properties identical to those of rhodopsin in the membrane of rod outer segments (ROS). Our solubilized rhodopsin spectra are in excellent agreement with the literature results (*36*, *37*), even when small concentrations [OD (λ_{max}) = 0.04] of protein are used. By using samples without lipids, scattering was significantly reduced.

Rhodopsin was also used as a control for the chromophore extraction experiments. Table 1 summarizes the low-temperature spectroscopy and chromophore extraction data. Retinal was extracted from bovine rhodopsin in the dark, and as expected, 95% of the retinal was found to be in the 11-cis conformation. This observation indicated that the experimental error of our method was roughly 5%. The bathochromic-shifted photostationary state (PSS458) produced by illuminating a 70 K rhodopsin sample at 458 nm was composed of 28% 11-*cis*-retinal, 58% *all-trans*-retinal, and 14% 9-*cis*-retinal. This comparison is in agreement with previously reported values (*37*, *38*). Furthermore, when the PSS458 was illuminated with 565 nm light to generate the photostationary state at 565 (PSS565), an isomeric composition was recovered consistent with literature data (11% 11-*cis*-retinal, 2% *all-trans*-retinal, and 87% 9-*cis*-retinal) (*37*, *38*). These results showed that our microvolumetric spectroscopic procedures could accurately reproduce low-temperature ROS rhodopsin spectra. Furthermore, the retinal extraction methods yielded isomeric distributions in good agreement with literature reports.

Low-Temperature Spectroscopy and Retinal Extraction of the Violet Cone Opsin. The low-temperature (30 and 70 K) violet cone opsin spectra are shown in Figure 3. Whereas the rhodopsin absorption maximum shifts during cooling to 77 K (*36*), the violet opsin absorption maximum displays no significant temperature dependence (Figure 3, curve 1). Upon incremental irradiation at 395 nm and 30 K, the protein absorption maximum shifts to higher wavelengths and broadens (Figure 3, curve 2). When the protein absorption spectrum no longer changes with additional illumination, a photostationary state (PSS) has been produced. The difference spectrum obtained by subtracting the original opsin spectrum from the PSS395 spectrum at 30 K is shown in the inset of Figure 3 (dot-dashed curve). The sample was then illuminated with light at 500 nm. The pigment reverted nearly identical to the original absorption spectrum (Figure 3, curve 3). When illuminated again with 395 nm light, an identical PSS395 was produced (Figure 3, curve 2). The violet opsin sample was then warmed to 70 K. The dark-adapted sample is identical to the curve shown in Figure 3 (curve 1). When illuminated at 395 nm, Figure 3, curve 4, was generated. This bathochromic photostationary state reconverted to curve 5 when illuminated with 500 nm light. The difference spectrum (spectrum 4 minus spectrum 1) is shown in the inset as the dashed spectrum.

Retinal was extracted from the violet cone opsin to characterize the isomeric composition of retinal in these

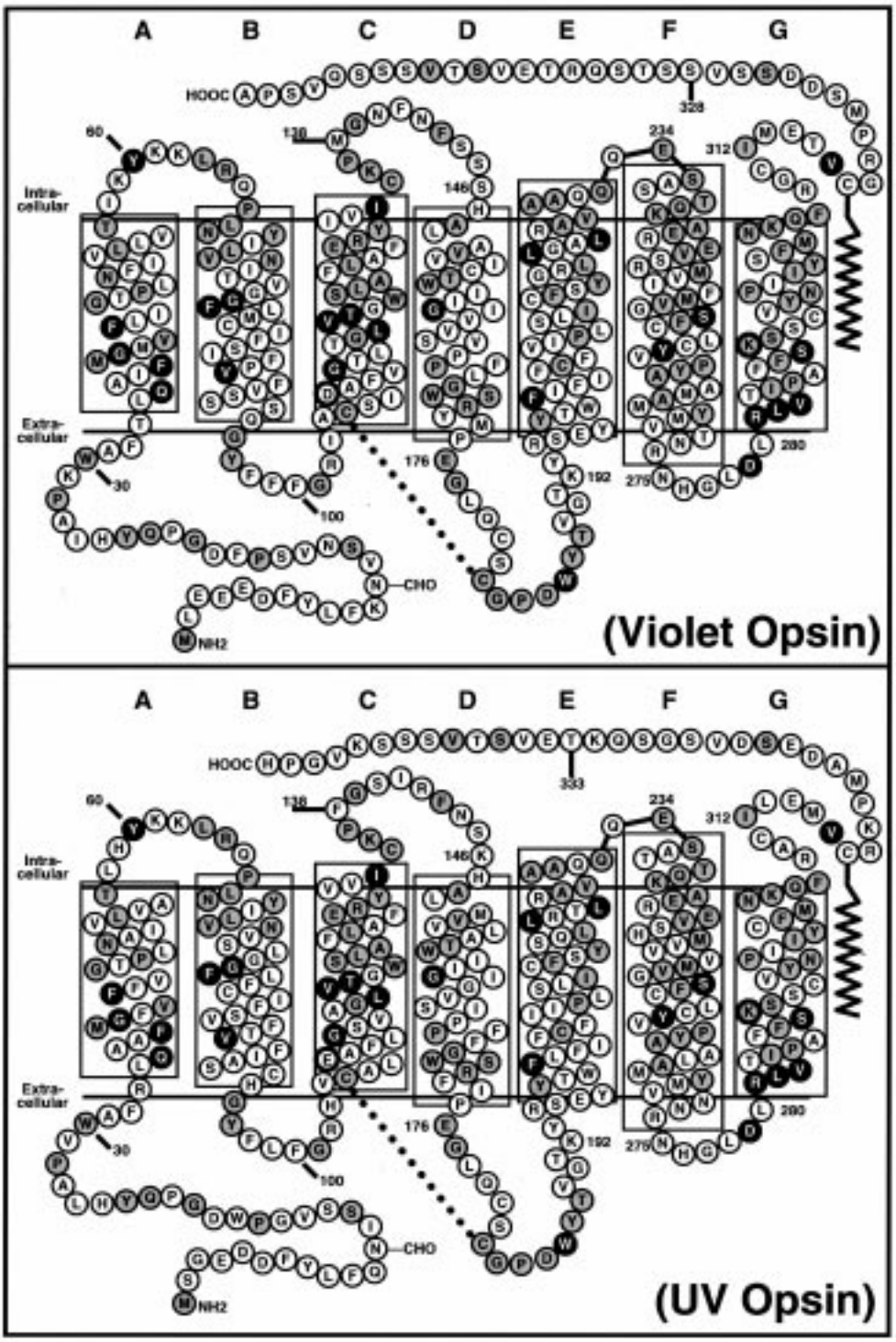

FIGURE 2: Primary sequences and putative secondary structures of the *X. laevis* violet-sensitive and mouse UV-sensitive cone opsins. The 20 full-length group S amino acid sequences available in GenBank (release 112.0, 6/99) were aligned against human rod opsin and human green cone opsin. Amino acids not identical to all group S sequences are unfilled. The 108 amino acids identical in all group S proteins and with the human rod and/or green cone opsins are shaded gray. The 26 amino acids shaded black (with white letters) are identical in the 20 group S opsins but are different from the human rod and green cone opsins. The proposed counterions (D108 for the violet opsin and E108 for UV opsin) and retinal binding sites (K291 for both proteins) are indicated with dark borders.

photostationary states. The results of the chromophore extraction are shown in Figure 4 and are summarized in Table 2. A sample of violet opsin was prepared as described for low-temperature spectroscopy. The sample was then cooled to 70 K, and a spectrum was recorded (Figure 3, curve 1). The retinal was extracted from this sample and the composition indicated 95% 11-*cis*-retinal, 5% *all-trans*-retinal, and less than 1% of 9-*cis*-retinal and other isomers. Thus, our low-temperature conditions do not cause significant dark isomerization. A chromophore extraction study of the batho-shifted photostationary state (PSS395) measured 12% (unchanged) 11-*cis*-retinal, 68% *all-trans*-retinal, and 20% 9-*cis*-retinal. Surprisingly, the reverse photostationary state (PSS500) was made up of 50% 11-*cis*-retinal, 11% *all-trans*-retinal, and 39% 9-*cis*-retinal. It is unclear why the spectrum of PSS500 is so similar to initial violet opsin, whereas the retinal

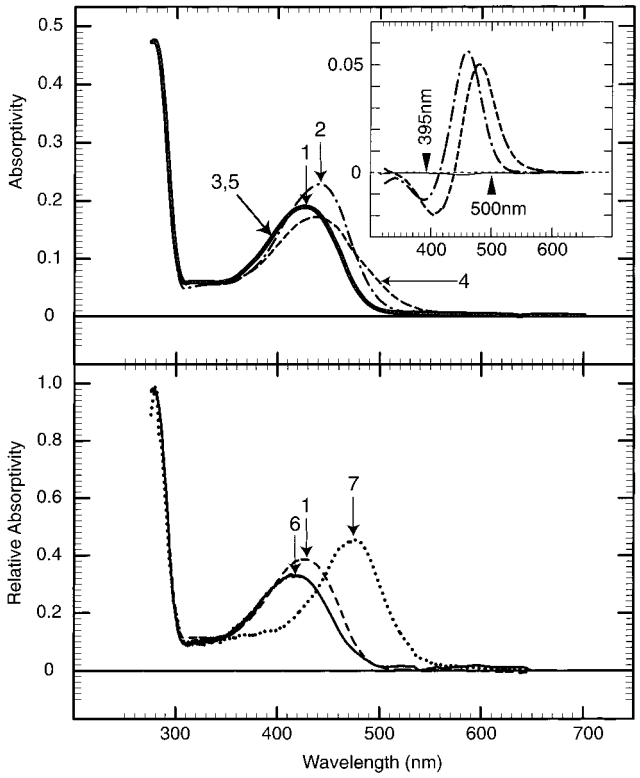

FIGURE 3: Low-temperature spectra of the violet cone opsin in 67% glycerol and 0.05% LM. In the top panel, spectrum 1 is the original sample (pure A_1 11-cis violet opsin) at 30 and 70 K, spectrum 2 is the 395 nm photostationary state generated at 30 K, spectra 3 and 5 are the 500 nm photostationary states at 30 and 70 K, and spectrum 4 is the 395 nm photostationary state at 70 K. The inset shows the difference spectra of spectrum 2 minus spectrum 1 (dot-dashed spectrum), spectrum 4 minus spectrum 1 (dashed spectrum), and spectrum 5 minus spectrum 1 (solid). The bottom panel shows spectrum 1 from above (dashed in lower panel), and spectrum 6 is 9-*cis*-retinal-regenerated violet opsin (isoviolet opsin). Spectrum 7 is a bathoviolet opsin spectrum calculated by addition of 20% of spectrum 6 (isoviolet opsin) and 12% of spectrum 1 (11-cis regenerated violet opsin) to the dashed difference spectrum from the inset above (spectrum 4 minus spectrum 1).

composition is so different. Using the HPLC data of the PSS395 and the spectra of the dark-adapted 11-cis generated violet opsin spectrum along with an experimentally determined 9-*cis*-retinal generated violet opsin spectrum (Figure 3, curve 6), the pure batho-violet opsin spectrum was calculated and yields a spectrum with a λ_{max} at 475 nm (Figure 3, curve 7).

Absorption of the Isoviolet Opsin. When illuminated at 77 K, rhodopsin, group L, and M_2 pigments form equilibria between the original protein (11-*cis*-retinal chromophore), the batho-pigment (*all-trans*-retinal chromophore), and the isopigment (9-*cis*-retinal chromophore). To determine the absorption maximum of the isoviolet opsin, violet cone apoprotein was regenerated with 9-*cis*-retinal. The resulting spectrum is shown in Figure 3 (curve 6; $\lambda_{max} = 415$ nm).

Cl^- Effect in the Violet Opsin. The spectroscopic and photochemical properties of the red and green cone opsins in both chickens and humans are influenced significantly by the binding of chloride ion to a specific site on the D−E extracellular loop of the protein (*30*, *39*−*41*). It has been argued, however, that the rhodopsins and the short-wavelength cone proteins do not have chloride binding sites (*41*). We studied the potential role of chloride ion on violet

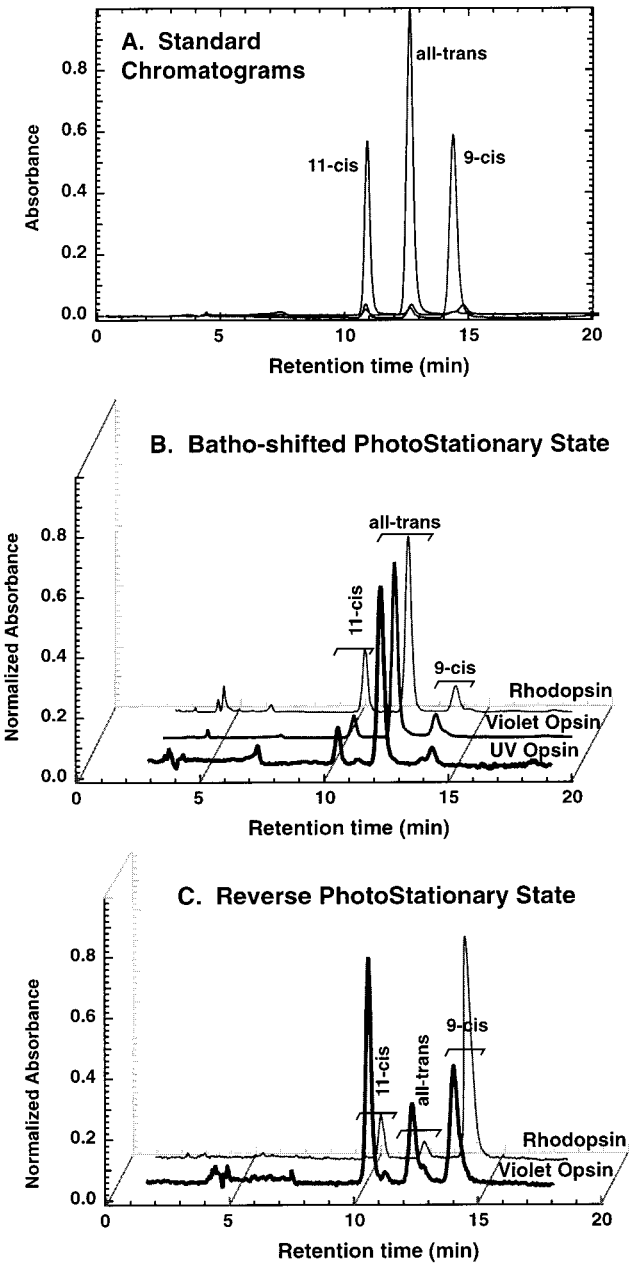

FIGURE 4: HPLC retinal oxime extraction data. Panel A shows an HPLC chromatogram of the 11-*cis*-, *all-trans*-, and 9-*cis*-retinal oxime standards. The chromatogram was run with equimolar amounts of each of the retinal oximes. The difference in peak areas arises from differences in the extinction coefficients. Panel B shows the chromatograms of the batho-shifted photostationary states of UV opsin and violet opsin. Bovine rhodopsin is included as a control. Panel C shows the chromatogram of the 500 nm photostationary state for violet opsin at 70 K. The 458 nm photostationary state for bovine rhodopsin at 70 K is shown for comparison. Panels B and C have the chromatograms shifted in space on the *x*- and *y*-axes for convenience, but the retention times are the same for each of the isomeric peaks.

opsin by monitoring the absorption spectrum as a function of chloride ion concentration. As shown in Table 2, chloride ion does not have a significant effect on the absorption spectrum other than a small absorption shift due to partial denaturation accompanying rigorous chloride ion removal. Thus, if violet opsin has a chloride binding site, occupation of this site has no spectroscopic consequences.

Low-Temperature Spectroscopy and Retinal Extraction of the UV Cone Opsin. The low-temperature (70 K) UV cone

Table 2: Spectroscopic and Chromophore Extraction Properties of *X. Laevis* Violet Cone Opsin

	T (K)	λ_{max} (nm)	ϵ (M^{-1} cm^{-1})	$\Delta\nu_{FWHM}$ (cm^{-1})	f [a]	ρ [a]	11-cis	all-trans	9-cis
WT (lit.)[b]	277	425	39400	5270			(100)[c]		
WT	277	426	(39400)	5220	0.99	1.60	95	5	0
WT (iso)	277	415		6180		1.81			(100)
Cl^- free	277	425		5300			(100)		
WT	70	424		5320	1.00	1.78	95	5	0
WT (iso)	70	410−416		6760		1.80			(100)
PSS395	70	435	N/A	5280	N/A	1.18	12	68	20
PSS500	70	425	N/A	5240	N/A	1.83	50	11	39
batho[d]	70	475		3340		1.31		(100)	

[a] See footnote *a* to Table 1. [b] References *10* and *25*. [c] Values in parentheses are assumed, not measured. [d] Calculated spectrum corresponding to the pure batho-violet cone (100% all-trans chromophore).

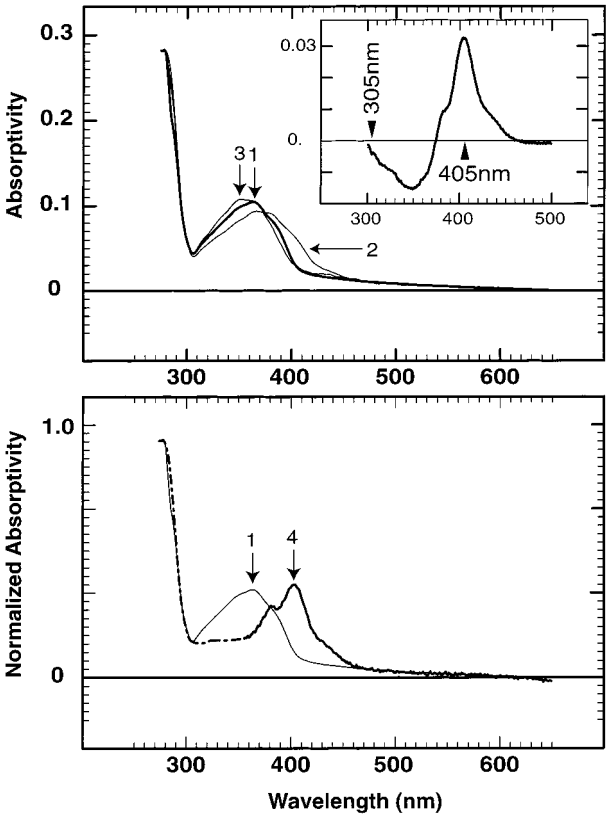

FIGURE 5: Low-temperature spectra of the mouse UV cone opsin in 67% glycerol and 0.05% LM. In the top panel, spectrum 1 is the mouse UV opsin at 70 K (initial state). Spectra 2 and 3 are the 305 and 405 nm photostationary states at 70 K, respectively. The inset is the difference spectrum of spectrum 2 minus spectrum 1. In the lower panel, curve 1 is shown from above for convenience, and curve 4 is the calculated mouse UV batho spectrum calculated from the difference spectrum and the chromophore extraction data given in Table 3. The blue edge of curve 4 is dashed to represent the uncertainty in that region of the spectrum because iso-UV (9-cis) opsin has not been generated and is estimated here (see text for details).

opsin spectra are shown in Figure 5. The mouse UV cone opsin samples were prepared for low-temperature spectroscopy as described above. Unlike the violet opsin, the UV cone opsin absorption band experiences an ~4 nm red absorption maximum shift and a broadening of 400 cm^{-1} upon cooling to 70 K (Figure 5, curve 1; see also Table 3). Once the sample has equilibrated at 70 K for 1 h, 305 nm light induced a bathochromic spectral shift (Figure 5, curve 2). This photostationary state (PSS305) was then illuminated with 405 nm light to produce a slight blue shift relative to the original spectrum (Figure 5, curve 3). To determine the spectral properties of the pure batho-UV opsin intermediate, retinal extraction was performed on the batho-shifted photostationary state of UV opsin (Figure 4B). PSS305 was found to have 20% 11-*cis*-retinal, 72% *all-trans*-retinal, and 8% 9-*cis*-retinal. The "pure" batho-UV spectrum (Figure 5, curve 4) was approximated by addition of 20% of the 11-*cis*-retinal spectrum of mouse UV (Figure 5, curve 1) back to the difference spectrum of PSS305 minus dark pigment (Figure 5, inset). Because so little iso-UV pigment is formed at 70 K (8%), and the spectral properties are probably very similar to those of dark-adapted UV opsin, the 9-cis component was neglected. The resulting spectrum of batho-UV is shown in Figure 5 (curve 4), and the region of uncertainty due to iso-pigment is shown using a dashed line.

Acid Denaturation of the UV Cone Opsin. The mouse UV-sensitive opsin was purified at pH 6.6 as described above and then incrementally acidified to pH 5.5, 4.3, 4.0, 3.6, and 1.8 with aliquots of 0.1 M H_2SO_4 at 4 °C. By using the extinction coefficient of 30 800 M^{-1} cm^{-1} for the acid-denatured (pH 1.8) retinal absorption maximum (Figure 6, λ_{max} = 440 nm), an extinction coefficient of 41 760 M^{-1} cm^{-1} was calculated for the UV-sensitive opsin (Figure 6, λ_{max} = 357 nm) (*42*). Thus, retinal must be covalently bound to the opsin. Furthermore, a single isosbestic point at 400 nm was generated by increasing the acidity of the protein solution (data not shown). If the initial (11-cis) state of UV opsin contains a deprotonated retinal Schiff base, decreasing the pH does not produce an apparent "protonated" retinal spectral shift.

DISCUSSION

This study represents the first low-temperature study of short-wavelength-sensitive cone opsins. To obtain sufficient protein quantities for this study, the genes for the violet-sensitive opsin from *X. laevis* and the UV-sensitive opsin from mouse were expressed transiently in mammalian COS1 cells. LM was used to solubilize the proteins in a solution with minimal scattering at low temperatures. Rhodopsin was used as a control in these experiments to confirm that LM does not shift the absorption maximum of species formed at 70 K. The difference spectrum of solubilized rhodopsin (postillumination minus preillumination at 70 K) is consistent with that reported in the literature (*37*, *38*). LM does not affect the spectra of the bathorhodopsin intermediate formed upon illumination at cryogenic temperatures. Furthermore, it probably does not affect the absorption spectra of the UV/violet opsins or their batho intermediates.

To determine whether our retinal extraction method induced (dark) retinal isomerization, bovine rhodopsin was

Table 3: Spectroscopic and Chromophore Extraction Properties of Mouse UV Cone Opsin

	T (K)	λ_{max} (nm)	ϵ (M^{-1} cm^{-1})	$\Delta\nu_{FWHM}$ (cm^{-1})	f [a]	ρ [a]	11-cis	all-trans	9-cis
WT	277	357	41760	6330	1.3	1.58	(100)[b]		
WT	70	361		6760		1.74	(100)		
PSS305	70	370		7120		1.48	20	72	8
PSS405	70	350							
batho[c]	70	403 (382)						(100)	

[a] See footnote *a* to Table 1. [b] Values in parentheses are assumed, not measured. [c] Calculated spectrum corresponding to the pure batho-UV cone (100% all-trans chromophore).

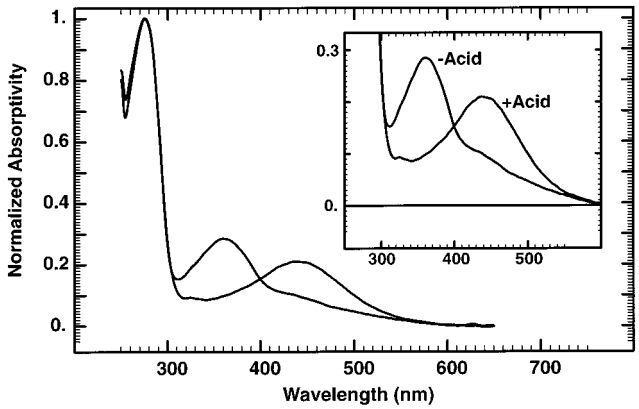

FIGURE 6: Mouse UV opsin at pH 6.6 and 4 °C is shown with a λ_{max} of 357 nm (−Acid). When sulfuric acid is added to pH 1.8 (+Acid), the λ_{max} is shifted to 440 nm, typical of a protonated Schiff base in solution.

used as a control. Photostationary states of rhodopsin were formed at 70 K with 458 and 565 nm light. Our results were in agreement with previously determined retinal isomeric concentrations (see Table 1). Furthermore, samples of the violet opsin and rhodopsin were prepared for low-temperature spectroscopy as described above and then cooled for 90 min to 70 K in the dark. The retinal was then extracted from these samples and found to consist of 95% 11-*cis*-retinal and 5% *all-trans*-retinal as quantitated by HPLC (see Tables 1 and 2). These results indicate that the extraction does not cause significant retinal isomerization in the dark.

The low-temperature spectroscopy of the violet opsin reveals two trappable bathochromic intermediates with different absorption spectra. The batho-violet state trapped at 30 K (XB_{30K}) has a $\lambda_{max} \approx 446$ nm, whereas the batho-violet state trapped at 70 K (XB_{70K}) has a $\lambda_{max} \approx 475$ nm. Two batho products have not been observed in any other vertebrate opsin. The possible origin of these different bathochromic states is discussed below. The reverse photostationary state spectrum of the violet opsin (PSS500) at 70 K (Figure 3, curves 3 and 5) is remarkably similar to the original dark spectrum of the violet opsin (Figure 3, curve 1), but the HPLC data show that it is quite different from the original (dark) pigment. PSS500 contains ∼40% 9-*cis*-retinal. This observation is possible because the extinction of the violet opsin regenerated with 9-*cis*-retinal is less than the 11-cis regenerated protein, and the blue edge of the isoopsin absorption overlaps with the blue edge of the 11-cis generated opsin (see Figure 3, curves 1 and 6). The absorption maximum of violet opsin is insensitive to chloride ion. Whereas chloride participates in the spectral tuning of the longer wavelength cone pigments, the violet opsin is insensitive to the presence of chloride ion (see Table 2).

This study is also the first cryogenic spectroscopic investigation of a UV-sensitive vertebrate opsin. When illuminated at 305 nm and 70 K, a bathochromic photostationary state is produced. By using HPLC analysis of the retinal extraction, a batho-UV opsin spectrum is calculated to have a $\lambda_{max} \approx 403$ nm. The batho-UV spectrum is unique in that it has a distinctive vibronic peak at 380 nm and the total absorption band is narrower than observed in the other opsins. These features suggest that the chromophore state or binding site environment is very different in this pigment and may indicate that the 11-cis chromophore is deprotonated. We examine the mechanism of wavelength tuning in more detail below.

The UV opsin was titrated with sulfuric acid to pH 1.8. At low pH, the absorption maximum shifted from 357 to 440 nm, representative of a bound protonated Schiff base retinal in solution. Therefore, the retinal must bind with mouse UV opsin to form a covalent linkage. Furthermore, from these data we were able to calculate the extinction coefficient of the mouse UV-sensitive opsin as ∼41 760 M^{-1} cm^{-1}. The titration also failed to produce an intermediate with any absorption maximum other than 357 and 440 nm. If the Schiff base linkage in mouse UV opsin is deprotonated, making the solution more acidic does not produce a state with an absorption maximum different from 440 nm.

The cryogenic batho-product difference spectra of four selected visual pigments are shown in Figure 7. We have normalized the difference spectra so that the absorptivity maximum is set to unity and then integrated under the positive and negative going bands:

$$I_{pos} = \int_{\tilde{\nu}_1}^{\tilde{\nu}_2} \mathrm{Norm}[\mathrm{PSS}_{\lambda_B}(\tilde{\nu}) - R(\tilde{\nu})]\, d\tilde{\nu} \qquad (1)$$

$$I_{neg} = \int_{\tilde{\nu}_2}^{\tilde{\nu}_3} \mathrm{Norm}[\mathrm{PSS}_{\lambda_B}(\tilde{\nu}) - R(\tilde{\nu})]\, d\tilde{\nu} \qquad (2)$$

where $\mathrm{PSS}_{\lambda_B}(\tilde{\nu})$ is the photostationary state induced by excitation at λ_B, $R(\tilde{\nu})$ is the spectrum of the initial (11-cis chromophore) state, Norm[x] represents the ($\lambda_{max} \rightarrow 1$) normalization function, and the frequency values $\tilde{\nu}_1$, $\tilde{\nu}_2$, and $\tilde{\nu}_3$ are defined in Figure 7. We note that while the assignment of $\tilde{\nu}_1$ and $\tilde{\nu}_2$ is straightforward, the assignment of $\tilde{\nu}_3$ can be problematic due to contributions of the higher energy band systems. We have included this source of error in the error bars but note that it is not of significance for the discussion that follows. The absolute values of the positive and negative integrals are plotted as a function of the difference spectrum frequency maxima in the lower panel of Figure 8. The upper panel of this figure shows the shift in the frequency of the absorption maximum between the (all-trans chromophore) batho photoproduct and the (11-cis) initial state. We have added additional pigments in both graphs for comparative purposes.

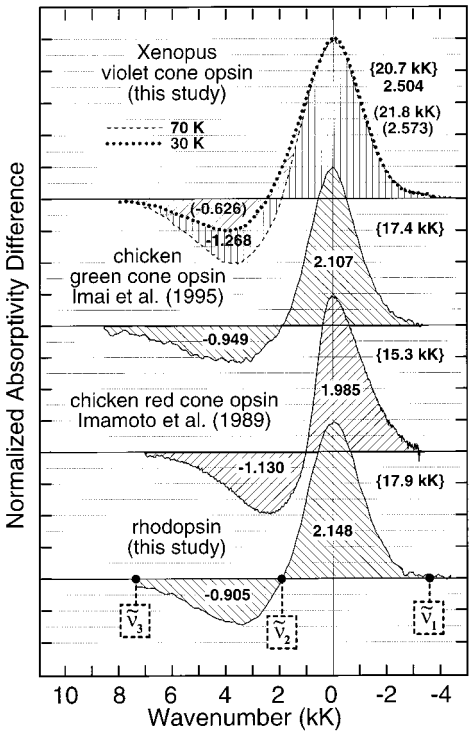

FIGURE 7: Comparison of the energy-shifted, normalized difference spectra of the bathochromic photoproduct photostationary states of rhodopsin (this study), chicken red cone opsin (*39*), chicken green cone opsin (*46*), and *X. laevis* violet cone opsin in 67% glycerol at 30 K (formation of XB_{30K}) and 70 K (formation of XB_{70K}) (see text for details). The difference spectra are relative to the starting material (pure A_1 11-cis pigment).

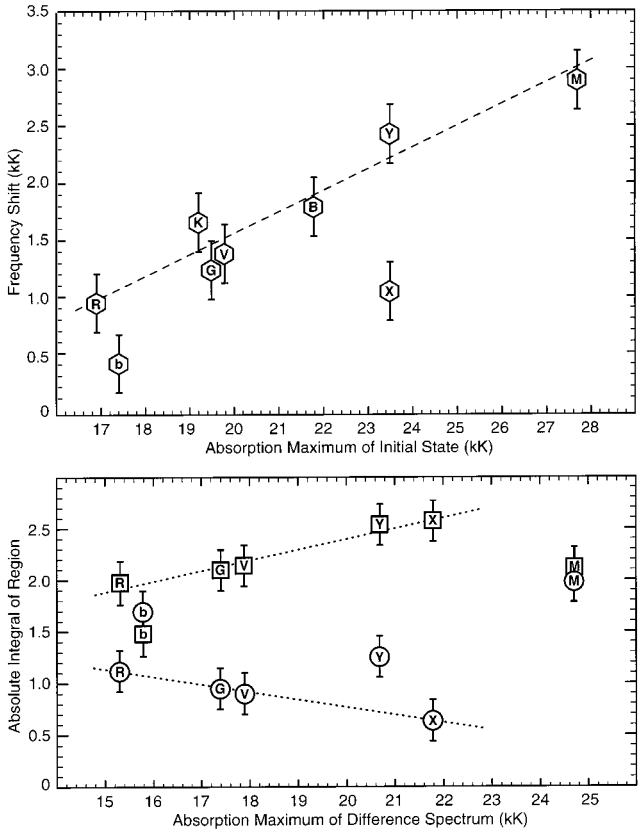

FIGURE 8: The top graph (A) plots the frequency shift associated with formation of the batho photoproduct (1 kK = 1000 cm^{-1}) versus the absorption maximum of the initial (11-cis A_1) protein. The bottom graph (B) compares the integrals of the positive and negative bands in the bathochromic difference spectra of selected pigments plotted versus the wavenumber of the peak absorptivity difference [I_{pos} (eq 1) in squares $-I_{neg}$ (eq 2) in circles]. The letters indicate the pigment and, where relevant, conditions: b = bacteriorhodopsin (light adapted), R = chicken red cone opsin (*39*), G = chicken green cone opsin (*46*), B = chicken blue cone opsin (*55*), V = bovine rhodopsin (this study), Y = *X. laevis* violet cone opsin at 70 K, X = *X. laevis* violet cone opsin at 30 K, M = mouse UV cone opsin, and K = Gecko green cone opsin (P521) (*56*).

Before analyzing these results, some features of the integral analysis deserve mention. First, the difference spectra have been generated by irradiating the protein at short wavelengths appropriate for maximizing conversion to form the primary, red-shifted photoproduct (or "batho" pigment). By normalizing the difference spectra, the band integrals are independent of the primary event quantum efficiency. These integrals are sensitive to the changes in both the frequency and shape of the initial and subsequent absorption spectra as well as the change in the oscillator strength of the λ_{max} band that accompanies the primary photochemical event. The error bars include the potential contribution of iso-pigment as well as errors associated with assignment of $\tilde{\nu}_3$ (see above). Using MNDO-PSDCI molecular orbital theory (*43*, *44*), we have simulated the changes in oscillator strength that accompany 11-cis to 11-trans photochemistry. The calculations indicate that 11-cis → 11-trans isomerization of the protonated Schiff base chromophore in the presence of a negative counterion yields isomerization-induced changes in the oscillator strength of the λ_{max} band that are very sensitive to the conformation of the 11-cis and 11-trans chromophores and the location of the counterion relative to the chromophore. This sensitivity is due to the fact that the lowest lying $^1B_u{}^{*+}$-like and second-excited $^1A_g{}^{*-}$-like π,π^* states both contribute to the λ_{max} band. The mixing of these states with one another, and the mixing of the $^1A_g{}^{*-}$-like state with higher energy states, is sensitive to the electrostatic fields inside the binding site (see discussion in ref *45*). Thus the integrals defined in eqs 1 and 2 provide a unique window on the mechanism of wavelength selection of the pigments under study.

Bovine rhodopsin, chicken red cone (*39*), chicken green cone (*46*), and the *X. laevis* violet cone opsins yield a set of positive and negative integrals that fall along two linear trend lines (provided that XB_{30K} is selected for the violet cone). We will refer to these proteins as being members of the primary group. We interpret this observation to mean that the change in oscillator strength of the bathorhodopsin photoproducts of the primary group pigments are changing in a systematic way that suggests a conserved mechanism for both wavelength selection and energy storage. This observation does not indicate that the binding sites of the primary group are identical but rather differ in going from red to green to violet via systematic changes in the position of the primary counterion relative to the protonated Schiff base. Because we know that the binding site of bovine rhodopsin is neutral and contains a single negatively charged counterion interacting with a positively charged protonated Schiff base chromophore (*45*), we conclude that this statement applies to all the primary group pigments. This observation suggests that the chloride ion that is critical for wavelength tuning in group L cone opsins carries out its function by indirectly stabilizing a protein conformation rather than entering the binding site and shifting the

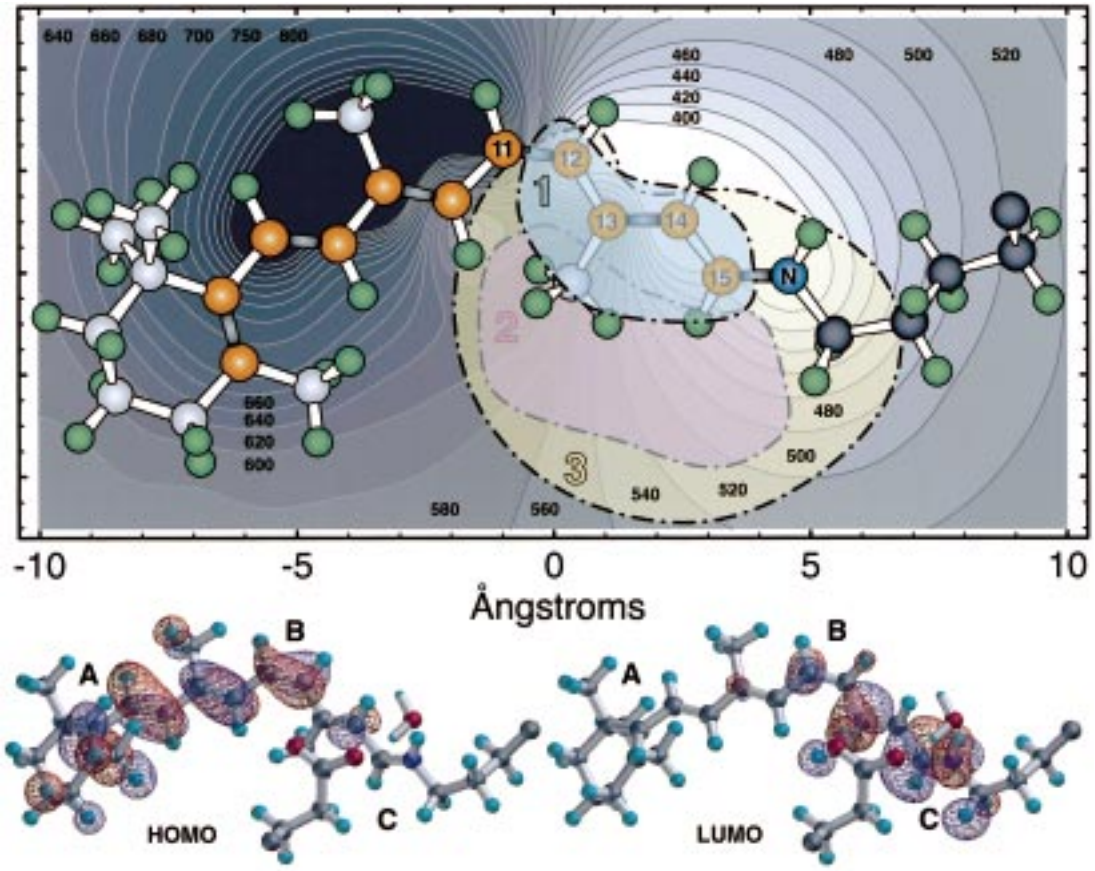

FIGURE 9: Theoretical analysis of counterion influence on the wavelength of the λ_{max} ($^1B_u{}^{*+} \leftarrow S_0$) absorption band (values in nanometers, solid bordered contours) and counterion location constraints (colored dashed contours labeled 1, 2, and 3) superimposed on the A_1 11-cis protonated Schiff base chromophore (see text). The $^1B_u{}^{*+}$ excited state is dominated by a single excitation homo → lumo transition (see text), and the molecular orbitals are shown in the insert below. A negative counterion located near position A will induce a red shift and near position C a blue shift. A counterion near position B will produce little if any shift. The solid line trends observed in Figure 8 can be reproduced only if the single counterion is constrained for all four pigments within regions 1 (above the chromophore) and 2 (in the plane of the chromophore) inclusive. Region 3 expands the in-plane constraints based on anticipated errors in our calculations. Absorption maxima from 400 to 570 and beyond can be accommodated on the basis of these constraints, but the counterion must be above or below the plane of the chromophore to generate absorption bands at wavelengths below 460 nm. These constraints do not apply if more than one counterion is within the binding site.

absorption maximum via direct electrostatic interaction with the chromophore.

Bacteriorhodopsin and mouse UV cone pigment do not belong to the primary group (Figure 8). We know from recent studies on bacteriorhodopsin that the counterion environment for this protein is quite different and is best represented as a quadrapole (see discussion in ref *43*). When coupled with the fact that the primary event involves an all-trans to 13-cis photoisomerization, it is not surprising that this pigment is not a member of the primary group. The fact that the mouse UV cone pigment does not belong to the primary group is more surprising, because it is in the same subgroup as the violet cone opsin [SWS1 based on Yokoyama's scheme (*3*)]. We may infer from the results of Figure 8 that wavelength mediation in mouse UV operates via a nonconserved, qualitatively different mechanism from that of the primary group. One possibility is that blue shifting of the mouse UV initial (11-cis) state is accomplished by adopting a deprotonated Schiff base chromophore. However, this possibility must be examined carefully in light of the batho-induced red-shift data shown in Figure 8A. We note that mouse UV exhibits a batho energy shift that obeys the same linear relationship that is observed for the set of pigments containing protonated Schiff base chromophores. It will be a challenge to explain how an ~2800 cm^{-1} red shift is induced upon isomerization of a nonprotonated Schiff base chromophore. One possibility is that the chromophore is unprotonated in the initial (11-cis chromophore) state and becomes protonated in response to electronic excitation either before or after photoisomerization. A comparable situation is observed for the back photochemical reaction of M (13-cis Schiff base) to bR (all-trans protonated Schiff base) in bacteriorhodopsin (*47*). Two-photon studies are underway to more fully examine the nature of the mouse UV cone binding site.

As noted above, *X. laevis* violet cone pigment has two bathorhodopsin photoproducts, one stable at 30 K (XB_{30K}) and one stable at 70 K (XB_{70K}). To our knowledge, no other visual pigment has two trappable batho photoproducts, although a full investigation of the effect of temperature on batho formation has likely not been carried out for many pigments. We note that XB_{30K} fits the integral trends of the primary group whereas XB_{70K} fits the frequency shift trends, which provides a perspective on the possible molecular origins. We suggest that XB_{30K} involves a distorted, blue-shifted chromophore due to significant steric interactions between the 11-trans chromophore and the protein. Energy storage in this species is primarily conformational, but upon

relaxation of the surrounding residues, a portion of the energy storage is transferred into charge separation to yield a more relaxed, but red-shifted photoproduct. This hypothesis is in keeping with our suggestion that the binding site of the *X. laevis* violet cone pigment is very compact relative to the other cone pigments.

We conclude with a more general discussion of the binding sites of the primary group, with an emphasis on the general mechanism of wavelength mediation. We have used MNDO-PSDCI molecular orbital calculations (*43*, *44*) to examine systematically the effect of counterion location on the absorption maxima for an 11-cis A_1 protonated Schiff base chromophore. The results are presented in Figure 9. The λ_{max} wavelength contours are drawn on the basis of the centroid of the negative charge on the single Glu or Asp counterion. The calculations indicate that the negative counterion can be manipulated to produce absorption maxima from 375 nm to well beyond 600 nm. The importance of counterion location on the spectroscopic properties of protonated Schiff bases has long been known (*48*) and has been viewed for many years as a primary determinant of pigment wavelength mediation (*49*, *50*). The data shown in Figure 9 indicate that it is thus possible to rationalize the wavelength mediation observed in the main group sequence entirely via manipulation of the counterion position. A calculation based on free minimization of the counterion yields a high blue-shifted species with an absorption maximum near 400 nm. Thus, the protein must constrain the counterion to higher energy positions further from the chromophore to achieve the wavelength maxima observed in the primary group. Our calculations suggest that the single negative counterion is located within region 3 of Figure 9 in the primary group.

Our prediction that all of the primary group pigments share a conserved mechanism does not preclude the selective introduction of amino acid residues into the binding site that perturb or enhance wavelength shifts via second-order mechanisms such as dispersion or dipole−dipole interactions. Dispersive red shifts can be induced by increasing the fraction of aromatic amino acids in close proximity to the chromophore. Dipole−dipole induced blue shifts are generated by increasing the fraction of hydroxyl-containing residues (Ser, Thr) or simply by increasing the amount of water near the chromophore. Our calculations indicate that each additional ROH residue (or water molecule) added to the first shell surrounding the chromophore induces a 200−400 cm^{-1} blue shift depending upon location, with the higher shifts generated by ROH (HOH) groups near the middle of the chromophore. Four strategically located groups would shift the absorption maximum of rhodopsin from 500 to ∼460 nm. Such a mechanism has been proposed for the blue cones by Lin et al. (*13*). Our conclusions are consistent with their models provided the major source of the wavelength tuning is associated with counterion location rather than hydroxyl enhancement. Two-photon (*45*, *51*, *52*) and photocalorimetric (*37*) studies are currently in progress to more accurately define the binding sites of the violet and UV cones studied here.

ACKNOWLEDGMENT

We thank Dr. Y. Shichida for providing us with digital versions of the published chicken red and green cone opsin difference spectra and Dr. J. Nathans for providing us with the mouse UV opsin cDNA. We also thank Dr. A. Surya for preparing solubilized rhodopsin and Mr. D. Singh and Drs. J. Stuart and E. Tan for interesting and helpful discussions.

REFERENCES

1. Schnapf, J., and Baylor, D. A. (1986) *Sci. Am. 256*, 32−39.
2. Yoshizawa, T. (1994) *Biophys. Chem. 50*, 17−24.
3. Yokoyama, S. (1995) *Mol. Biol. Evol. 12*, 53−61.
4. Okano, T., Kojima, D., Fukada, Y., Shichida, Y., and Yoshizawa, T. (1992) *Proc. Natl. Acad. Sci. U.S.A. 89*, 5932−5936.
5. Yokoyama, R., and Yokoyama, S. (1990) *Vision Res. 30*, 807−816.
6. Blatz, P. E., Johnson, R. H., Mohler, J. H., Al-Dilaimi, S. K., Dewhurst, S., and Erickson, J. O. (1971) *Photochem. Photobiol. 13*, 237−245.
7. Yokoyama, S., Radlwimmer, F. B., and Kawamura, S. (1998) *FEBS Lett. 423*, 155−158.
8. Jacobs, G. H., Deegan, G. F., and Neitz, J. (1998) *Visual Neurosci. 15*, 581−584.
9. Chiu, M. I., Zack, D. J., Wang, Y., and Nathans, J. (1994) *Genomics 21*, 440−443.
10. Starace, D. M., and Knox, B. E. (1998) *Exp. Eye Res. 67*, 209−220.
11. Archer, S., and Hirano, J. (1996) *Proc. R. Soc. London B, Biol. Sci. 263*, 761−767.
12. Baldwin, P., and Hubbell, W. (1993) *EMBO J. 12*, 1693−1703.
13. Lin, S. W., Kochendoerfer, G. G., Caroll, K. S., Wang, D., Mathies, R. A., and Sakmar, T. P. (1998) *J. Biol. Chem. 273*, 24583−24591.
14. Kochendoerfer, G. G., Wang, Z., Oprian, D. D., and Mathies, R. A. (1997) *Biochemistry 36*, 6577−6587.
15. Wilkie, S. E., Vissers, P. M. A. M., Das, D., DeGrip, W. J., Bowmaker, J. K., and Hunt, D. M. (1998) *Biochem. J. 330*, 541−547.
16. Chang, B. S. W., Crandall, K. A., Carulli, J. P., and Hartl, D. L. (1995) *Mol. Phylogenet. Evol. 4*, 31−43.
17. Yokoyama, S., and Zhang, H. (1997) *Gene 202*, 89−93.
18. Yoshizawa, T., and Kuwata, O. (1991) *Photochem. Photobiol. 54*, 1061−1070.
19. Calderone, J. B., and Jacobs, G. H. (1995) *Visual Neurosci. 12*, 463−468.
20. Okano, T., Fukada, Y., Artamonov, I. D., and Yoshizawa, T. (1989) *Biochemistry 28*, 8848−8856.
21. Merbs, S., and Nathans, J. (1992) *Science 258*, 464−466.
22. Merbs, S., and Nathans, J. (1992) *Photochem. Photobiol. 56*, 869−881.
23. Merbs, S., and Nathans, J. (1992) *Nature 356*, 443−435.
24. Kawamura, S., and Yokoyama, S. (1997) *Vision Res. 38*, 37−44.
25. Starace, D. M., and Knox, B. E. (1997) *J. Biol. Chem. 272*, 1095−1100.
26. Oprian, D. D., Asenjo, A. B., Lee, N., and Pelletier, S. L. (1991) *Biochemistry 30*, 11367−11372.
27. Oprian, D., Molday, R., Kaufman, R., and Khorana, G. (1987) *Proc. Natl. Acad. Sci. U.S.A. 84*, 8874−8879.
28. Khorana, H. G., Knox, B. E., Nasi, E., Swanson, R., and Thompson, D. A. (1988) *Proc. Natl. Acad. Sci. U.S.A. 85*, 7917−7921.
29. Molday, R. S., and MacKenzie, D. (1983) *Biochemistry 22*, 653−660.
30. Tachibanaki, S., Imamoto, Y., Imai, H., and Shichida, Y. (1995) *Biochemistry 34*, 13170−13175.
31. DeGrip, W. J. (1982) in *Methods in Enzymology*, pp 197−207, Academic Press, Inc., New York.
32. Imamoto, Y., Yoshizawa, T., and Shichida, Y. (1996) *Biochemistry 35*, 14599−14607.
33. Groenendijk, G. W. T., De Grip, W. J., and Daemen, F. J. M. (1980) *Biochim. Biophys. Acta 617*, 430−438.

34. Landers, G. M., and Olson, J. A. (1988) *J. Chromatogr. 438*, 383−392.
35. Groenendijk, G. W. T., Jansen, P. A. A., Bonting, S. L., and Daemen, F. J. M. (1980) in *Methods in Enzymology*, pp 203−220, Academic Press, Inc., New York.
36. Yoshizawa, T., and Shichida, Y. (1982) in *Methods in Enzymology*, pp 333−354, Academic Press, Inc., New York.
37. Schick, G. A., Cooper, T. M., Holloway, R. A., Murray, L. P., and Birge, R. R. (1987) *Biochemistry 26*, 2556−2562.
38. Suzuki, T., and Callender, R. H. (1981) *Biophys. J. 34*, 261−265.
39. Imamoto, Y., Kandori, H., Okano, T., Fukada, Y., Shichida, Y., and Yoshizawa, T. (1989) *Biochemistry 28*, 9412−9416.
40. Lewis, J. W., Liang, J., Ebrey, T. G., Sheves, M., and Kliger, D. S. (1995) *Biochemistry 34*, 5817−5823.
41. Wang, Z., Asenjo, A. B., and Oprian, D. D. (1993) *Biochemistry 32*, 2125−2130.
42. Kito, Y., Suzuki, T., Azuma, M., and Sekoguti, Y. (1968) *Nature 218*, 955−957.
43. Kusnetzow, A., Singh, D. L., Martin, C. H., Barani, I., and Birge, R. R. (1999) *Biophys. J. 78*, 2370−2389.
44. Martin, C. H., and Birge, R. R. (1998) *J. Phys. Chem. A 102*, 852−860.
45. Birge, R. R., Murray, L. P., Pierce, B. M., Akita, H., Balogh-Nair, V., Findsen, L. A., and Nakanishi, K. (1985) *Proc. Natl. Acad. Sci. U.S.A. 82*, 4117−4121.
46. Imai, H., Imamoto, Y., Yoshizawa, T., and Shichida, Y. (1995) *Biochemistry 34*, 10525−10531.
47. Stuart, J. A., and Birge, R. R. (1996) in *Biomembranes* (Lee, A. G., Ed.) pp 33−140, JAI Press, London.
48. Blatz, P. E., Mohler, J. H., and Navangul, H. V. (1972) *Biochemistry 11*, 848−855.
49. Honig, B., Dinur, U., Nakanishi, K., Balogh-Nair, V., Gawinowicz, M. A., Arnaboldi, M., and Motto, M. G. (1979) *J. Am. Chem. Soc. 101*, 7084−7086.
50. Kakitani, H., Kakitani, T., Rodman, H., and Honig, B. (1985) *Photochem. Photobiol. 41*, 471−479.
51. Birge, R. R. (1986) *Acc. Chem. Res. 19*, 138−146.
52. Stuart, J. A., Vought, B. W., Zhang, C. F., and Birge, R. R. (1995) *Biospectroscopy 1*, 9−28.
53. Birge, R. R. (1990) *Biochim. Biophys. Acta 1016*, 293−327.
54. Hisatomi, O., Satoh, T., Barthel, L. K., Stenkamp, D. L., Raymond, P. A., and Tokunga, F. (1996) *Vision Res. 36*, 933−939.
55. Imai, H., Terakita, A., Tachibanaki, S., Imamoto, Y., Yoshizawa, T., and Shichida, Y. (1997) *Biochemistry 36*, 12773−12779.
56. Kojima, D., Imai, H., Okano, T., Fukada, Y., Crescitelli, F., Yoshizawa, T., and Shichida, Y. (1995) *Biochemistry 34*, 1096−1106.

BI990968B